Multiaxial fatigue life prediction using an improved SWT model

Jing Li [a,b,*] *Feng-shan Shao* [a] *Zheng-wei He* [a] *Juan Ma* [a,b] *Yuan-ying Qiu* [a] *Michael Beer* [c]

[a] The Joint Laboratory for International Cooperation in Structural Mechanics of Composite Materials for Electronic Devices, School of Mechano-Electronic Engineering, Xidian University, No. 2 South Taibai Road, Xi'an, China, 710071

[b] Shaanxi Key Laboratory of Space Extreme Detection, Xidian University, No. 2 South Taibai Road, Xi'an, China, 710071

[c] Institute for Risk and Reliability, Faculty of Civil Engineering and Geodetic Science, Leibniz Universität Hannover, Callinstr. 34, Hannover, Germany, 30900

Abstract:

In this paper, the SWT model was improved by incorporating the Walker equation into the strain-life curve. The established model takes into account the material's sensitivity to mean stress by introducing the Walker exponent, *w*. Under uniaxial loading condition, the proposed model can reduce to the SWT model, Manson-Coffin equation, and Walker model for *w* values of 0.5, 1, and 0, respectively. Under multiaxial symmetric loading, when $w = 0.5$, the proposed model can be simplified as another SWT correction model (CXH) proposed by Chen et al. The prediction accuracy of the established model was validated using about 200 data points collected from literature. These data points were obtained from tests conducted on eight different kinds of metals under various multiaxial loading paths. The verification results indicate that 96.8% and 97.9% of the data points fall within the factor-of-three boundary for the loading paths without and with mean stresses, respectively.

Key words: Multiaxial cyclic loading, Walker exponent, Fatigue life prediction, SWT model, Strain energy density

* Corresponding author
E-mail address: lijing02010303@163.com (J. Li), Fax: +86 02984786547, Tel: +86 02984786693

1. INTRODUCTION

In service, many engineering structures are subjected to multiaxial cyclic loading, which may lead to multiaxial fatigue failures in metallic structures. Therefore, multiaxial fatigue failure is a well-known technical problem for metallic structures. The multiaxial fatigue cyclic load is typically defined as the generation of a stress state tensor on the loaded object at specific locations, where the stress tensor consists of two or more components. This may occur when multiple fatigue cyclic loads are applied, which may not necessarily be in-phase or proportional.[1-2] Accordingly, it is meaningful to estimate the multiaxial fatigue lives of structures, especially for that under non-proportional loading conditions.

As for multiaxial loading, many fatigue life estimation criteria have been developed in different expressions. Most of these models can be divided into the following four categories, i.e., stress-based approaches,[3-8] strain-based approaches,[9-15] strain-energy-based approaches,[16-24] and fracture mechanics approaches.[25-30] Among these fatigue life prediction models, those that combine the concept of critical plane and strain energy density are considered highly advanced for estimating multiaxial fatigue life of materials.[23] One of the widely-used fatigue life prediction models that belongs to this category was developed by Socie,[24] which is usually named as the SWT model. In this model, the critical plane was defined as the plane with the maximum range of tensile strain.[24] The SWT model is commonly used to estimate the fatigue lifetime of material that is mainly characterized by mode I crack propagation (tensile cracking).[24] In order to take into account the general cracking behavior, the SWT model was corrected by Jiang et al.[31-32] through introducing a material constant. The value of the introduced material constant varies depending on the cracking behavior. Unfortunately, it is a complex task to determine this material constant reasonably, especially in the absence of the test data. Chen et al.[33] (CXH) introduced the shear strain energy density into the SWT model based on the observation that the effect of shear terms on fatigue life is significant under 90° out-of-phase loading. However, the effect of mean stress is not taken into account in the CXH model, which may result in non-conservative predictions under asymmetric cyclic loading conditions. The SWT model was also corrected by Li et al.[34-35] through introducing the shear components. However, it fails to consider the different effects of shear and normal terms on

fatigue damage. Lv et al.[36] modified the SWT model by introducing a material-dependent exponent proposed by Walker.[37] According to Lv's proposal, the prediction accuracy can be improved by using their modified model. However, the shear components were also not considered in this modified method, which is similar to the SWT model. Kujawski[38] proposed a deviatoric SWT model to take into account the effect of negative mean stress on fatigue life. However, more multiaxial fatigue test data are necessary to verify the reliability of this model. Based on the idea of SWT, Ince and Glinka[39] suggest that both mean normal stress and mean shear stress only influence the elastic components. They therefore proposed two fatigue life prediction models, named as the GSE model and GSA model, respectively. Different from the SWT model, the critical plane in both models was defined as the maximum damage plane.[39] Subsequently, Ince[40] adopted the idea of Kujawski[38] and extended the GSE model to consider the influence of negative mean stress on fatigue life. Yu and his co-workers[41] believed that both the plastic and elastic terms are affected by shear and normal mean stresses. As a result, modifications were made to both the GSE and GSA models.[41] In contrast to the models proposed by Ince and Glinka[39], the critical plane in the two modified models was defined as the plane with the maximum shear strain.[41] Later, Yu's modified GSE model was improved by Li et al.[42] through considering the different effects of normal strain energy density and shear strain energy density on fatigue damage.

Most recently, 14 critical plane models were validated and compared by Poczklán et al.[43] using the experimental data of 316L steel tested under different loading paths. It was observed that the orientations of the cracks were the most accurately predicted by the SWT model, while the model proposed by Fatemi and Socie (FS)[44] presented the least accurate results. However, the predicted lifetime of FS model is the most satisfactory, where more than 93% of the data points fall within the factor-of-two boundary. In contrast, the life prediction results of the SWT model are far less accurate than those of the FS model. Nascimento et al.[45] performed strain-controlled tension, torsion and proportional fatigue experiments on Inconel 718 at 20℃ and 450℃, respectively. It was also found that, at both temperatures, the FS model presented more accurate fatigue life prediction results than the SWT model. The multiaxial notch fatigue behavior of 18Ni300 maraging steel produced by selective laser melting was studied by Branco et al.[46] through performing proportional bending-torsion tests with different

bending moment to torsion moment ratios. In the linear-elastic framework, a straightforward method was developed to estimate the multiaxial notch fatigue life of this material. This approach combines the SWT model with the theory of critical distances. The multiaxial fatigue behavior of A356-T6 aluminum alloy was studied by Nourian-Avval and Fatemi[47] through conducting a series of stress-controlled fatigue tests under various loading conditions, including axial, torsion, proportional, and non-proportional loadings. The study revealed that fatigue cracks propagated on the maximum normal stress plane in all tested conditions for A356-T6 aluminum alloy. However, the application of the SWT model for fatigue life prediction resulted in non-conservative estimates under non-proportional loadings.

Overall, while numerous criteria for estimating fatigue life have been developed, there is currently a lack of widely accepted models.[39] One possible reason for this is that the issue of converting multiaxial stress states to uniaxial equivalents has not been adequately addressed.[23] Therefore, in the present paper, the SWT model was improved by incorporating the equation of Walker into the strain-life curve. Step-by-step procedures were provided to determine the location of the maximum normal strain range plane and the damage parameters acting on this plane. The prediction accuracy of the established model was validated using about 200 data points collected from literature that were tested by eight kinds of metals under different multiaxial loading paths without/with mean stresses. Comparisons with the CXH, SWT and FS models showed that the established criterion gives the best prediction results in the considered loading paths regardless of whether the mean stresses are zero or not.

2. MODIFICATION OF THE SWT MODEL

2.1 Establishment of the life estimation model

Smith et al.[48] proposed that the fatigue damage of material was determined by the geometric mean of the stress amplitude and the maximum stress, and the following model was developed:

$$\sigma_{eq} = \sqrt{\sigma_{\max}\sigma_a} \tag{1}$$

where $\sigma_{\max}$ is the maximum stress, σ_a is the stress amplitude, and σ_{eq} is the equivalent completely reversed stress amplitude. Here, Eq. (1) is referred to as the Original SWT

(OSWT) model. This terminology is used to distinguish it from the multiaxial version of the SWT model developed by Socie.[24]

In reference,[37] a similar model was proposed by Walker. In this model, an additional material constant was introduced to account for the sensitivity of the material to mean stress. It can be presented as:

$$\sigma_{eq} = \sigma_{\max}^{1-w}\sigma_a^{w} \tag{2}$$

where w is the additional material constant named as Walker exponent. It can be determined by using the procedures proposed by Dowling.[49] In the absence of the test data, the Walker exponent can also be estimated by[6]:

$$w = \log_2 \frac{\sigma_0}{\sigma_{-1}} \tag{3}$$

where σ_0 and σ_{-1} represent the fatigue limits tested under repeating loadings with stress ratios R = 0 and -1, respectively. Equation (2) shows that the OSWT model is a special case of the Walker model. In other words, the Walker model reduces to the OSWT model as long as w = 0.5.

For completely reversed loading, the Basquin model is typically used to describe the stress-life curves. This model can be given by:

$$\sigma_a = \sigma_f' \left(2N_f\right)^b \tag{4}$$

where σ_f' is the fatigue strength coefficient, and b is the fatigue strength exponent. N_f is the fatigue life. For uniaxial fatigue loading with non-zero mean stress, the following equation was proposed by Dowling et al.[49-50] to describe the stress-life curve based on the equivalent stress amplitude and the Basquin equation:

$$\sigma_{eq} = \sigma_f' \left(2N_f\right)^b \tag{5}$$

For the completely reversed experiments, the strain-life curves are often described by the Coffin-Manson equation:

$$\varepsilon_{a,t} = \varepsilon_{a,e} + \varepsilon_{a,p} = \frac{\sigma_f'}{E}\left(2N_f\right)^b + \varepsilon_f' \left(2N_f\right)^c \tag{6}$$

where ε_f' and c are fatigue ductility coefficient and fatigue ductility exponent, respectively.

$\varepsilon_{a,p}$, $\varepsilon_{a,e}$, and $\varepsilon_{a,t}$ are the plastic, elastic and total strain amplitudes, respectively. E is the modulus of elasticity.

Substitute Eq. (2) into Eq. (5), the following equation can be derived:

$$\sigma_{\max}^{\frac{1-w}{w}}\sigma_a = \sigma_f'^{\frac{1}{w}}\left(2N_f\right)^{\frac{b}{w}} \tag{7}$$

If the material deformation is elastic, Eq. (7) can be rewritten as:

$$\sigma_{\max}^{\frac{1-w}{w}}E\varepsilon_{a,e} = \sigma_f'^{\frac{1}{w}}\left(2N_f\right)^{\frac{b}{w}} \tag{8}$$

Then,

$$\sigma_{\max}^{\frac{1-w}{w}}\varepsilon_{a,e} = \frac{\sigma_f'^{\frac{1}{w}}}{E}\left(2N_f\right)^{\frac{b}{w}} \tag{9}$$

If the material deformation is plastic, the relationship between $\varepsilon_{a,p}$ and σ_a can be described by the Ramberg-Osgood equation, that is:

$$\sigma_a = K'\varepsilon_{a,p}^{n'} \tag{10}$$

where K' is the cyclic strength coefficient, and n' is the cyclic strain hardening exponent. Substitute Eq. (10) into Eq. (7), Eq. (7) can be rewritten as:

$$\sigma_{\max}^{\frac{1-w}{w}}K'\varepsilon_{a,p}^{n'} = \sigma_f'^{\frac{1}{w}}\left(2N_f\right)^{\frac{b}{w}} \tag{11}$$

And then, the following equation can be obtained by substituting Eq. (6) into Eq. (11):

$$\sigma_{\max}^{\frac{1-w}{w}}\varepsilon_{a,p} = \frac{\sigma_f'^{\frac{1}{w}}}{K'}\left(2N_f\right)^{\frac{b}{w}}\varepsilon_{a,p}^{1-n'} = \frac{\sigma_f'^{\frac{1}{w}}}{K'}\varepsilon_f'^{1-n'}\left(2N_f\right)^{\frac{b}{w}+(1-n')c} \tag{12}$$

Based on Eqs. (9) and (12), an effective strain energy density model that is similar to the SWT model can be obtained:

$$\sigma_{\max}^{\frac{1-w}{w}}\varepsilon_{a,t} = \frac{\sigma_f'^{\frac{1}{w}}}{E}\left(2N_f\right)^{\frac{b}{w}} + \frac{\sigma_f'^{\frac{1}{w}}}{K'}\varepsilon_f'^{1-n'}\left(2N_f\right)^{\frac{b}{w}+(1-n')c} \tag{13}$$

The developed criterion, as represented by Eq. (13), can be directly used to evaluate the fatigue lifetime of a material under uniaxial loading conditions. In order to extend this equation for predicting the multiaxial fatigue lifetime of a material, the critical plane concept can be employed which is similar to the idea proposed by Socie.[24] Here, the critical plane was also defined as the plane of maximum normal strain range. Then, Eq. (13) can be rewritten as:

$$\sigma_{1,\max}^{\frac{1-w}{w}}\frac{\Delta\varepsilon_{1,\max}}{2}=\frac{\sigma_f'^{\frac{1}{w}}}{E}\left(2N_f\right)^{\frac{b}{w}}+\frac{\sigma_f'^{\frac{1}{w}}}{K'}\varepsilon_f'^{1-n'}\left(2N_f\right)^{\frac{b}{w}+(1-n')c} \tag{14}$$

where $\sigma_{1,\max}$ and $\Delta\varepsilon_{1,\max}$ are the maximum normal stress and the maximum normal strain range acting on the defined critical plane, respectively. Similar to the SWT model, Eq. (14) only takes into account the effect of normal terms on fatigue life. However, Chen et al.[33] have pointed out that both the shear stress and shear strain are significant on the maximum normal strain range plane under circular loading path, so that the shear terms should be taken into account for assessing the non-proportional fatigue life of material.

Taking 16MnR steel[51] for example, the relationships between the phase shift and various factors, including shear stress range, shear strain range, normal stress range, and normal strain range, acting on the maximum normal strain range plane were plotted in Fig. 1. Figure 1 illustrates that as the phase shift increases, the normal stress and strain ranges decrease, while the shear stress and strain ranges increase. The variations of shear and normal strain energy densities with the phase shift were illustrated in Figs. 2 and 3, respectively. These figures clearly show that the ratio of shear strain energy density to total strain energy density increases with the increase of the phase shift. More exactly, the shear strain energy accounts for about 40% of the total strain energy when the phase shift is 90°. Therefore, the shear strain energy density cannot be ignored for the out-of-phase loadings.

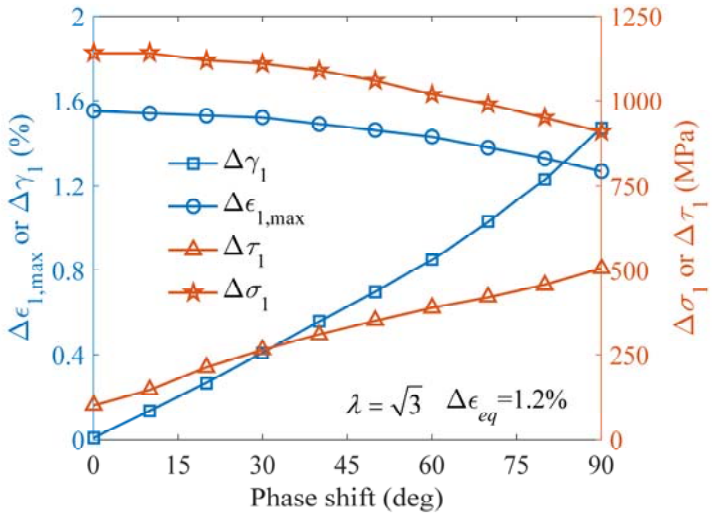

Fig. 1 Variations of stress and strain ranges with phase shift

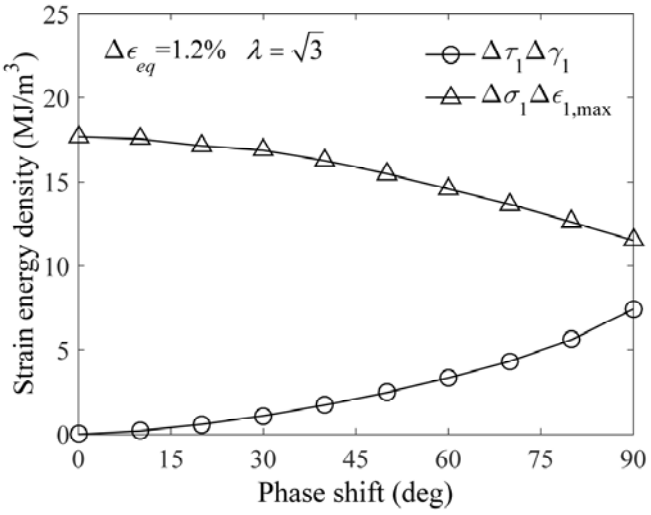

157

158 Fig. 2 Correlations between the strain energy density and phase shift

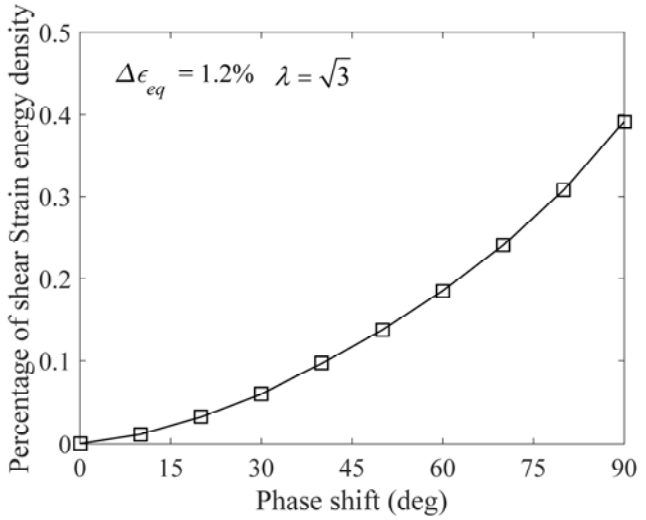

159

160 Fig. 3 Correlation between the percentage of shear strain energy density and phase shift

161 In reference,[52] multiaxial fatigue experiments were conducted by Itoh and his co-workers
162 on 304 stainless steel under the different loading paths. Here, the shear and normal strain
163 ranges as well as the shear and normal strain energy densities were calculated for the loading
164 paths shown in Fig. 4. Variation of the $\Delta\gamma_1/\Delta\varepsilon_{1,\max}$ with the non-proportionality factor was
165 illustrated in Fig. 5(a). In this figure, the non-proportionality factors for the loading paths
166 shown in Fig. 4 were determined using the test data. These non-proportionality factors have
167 been listed in reference.[53] It can be seen that, the value of $\Delta\gamma_1/\Delta\varepsilon_{1,\max}$ equals to 0 for pro-
168 portional loading. It means that there is only normal strain range acting on the maximum
169 normal strain range plane which is consistent with the Chen's observation.[33] However, the

ratios of $\Delta\gamma_1/\Delta\varepsilon_{1,\max}$ increase as the non-proportionality factors for non-proportional cyclic loadings increase. Figure 5(b) shows the variation of $\Delta\tau_1\Delta\gamma_1/\Delta\sigma_1\Delta\varepsilon_{1,\max}$ with the factor of non-proportionality. It can also be observed that the ratios of $\Delta\tau_1\Delta\gamma_1/\Delta\sigma_1\Delta\varepsilon_{1,\max}$ increase with increasing the factor of non-proportionality. Therefore, the shear terms acting on the maximum normal strain range plane should be considered under non-proportional loadings. For this reason, Eq. (14) was modified as:

$$\sigma_{1,\max}^{\frac{1-w}{w}}\frac{\Delta\varepsilon_{1,\max}}{2}+\left(\frac{\Delta\tau_1}{2}+\left|\tau_{1,m}\right|\right)^{\frac{1-w}{w}}\frac{\Delta\gamma_1}{2}=\frac{\sigma_f'^{\frac{1}{w}}}{E}\left(2N_f\right)^{\frac{b}{w}}+\frac{\sigma_f'^{\frac{1}{w}}}{K'}\varepsilon_f'^{1-n'}\left(2N_f\right)^{\frac{b}{w}+(1-n')c} \tag{15}$$

where $\tau_{1,m}$ represents the mean shear stress on the maximum normal strain range plane. Here, the introduction of $\left|\tau_{1,m}\right|$ is based on the reason that both the negative mean shear stress and the positive mean shear stress have similar detrimental effects on fatigue life.[54-56] Equation (15) named as N-SWT model shows that the proposed criterion not only takes into account the influence of both shear and normal components on fatigue damage, but also considers the sensitivity of the material to mean stress.

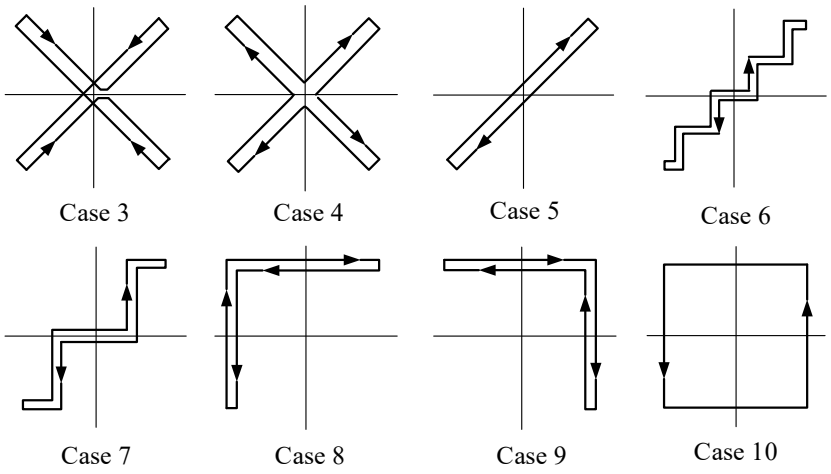

Fig. 4 The loading paths for 304 stainless steel[52]

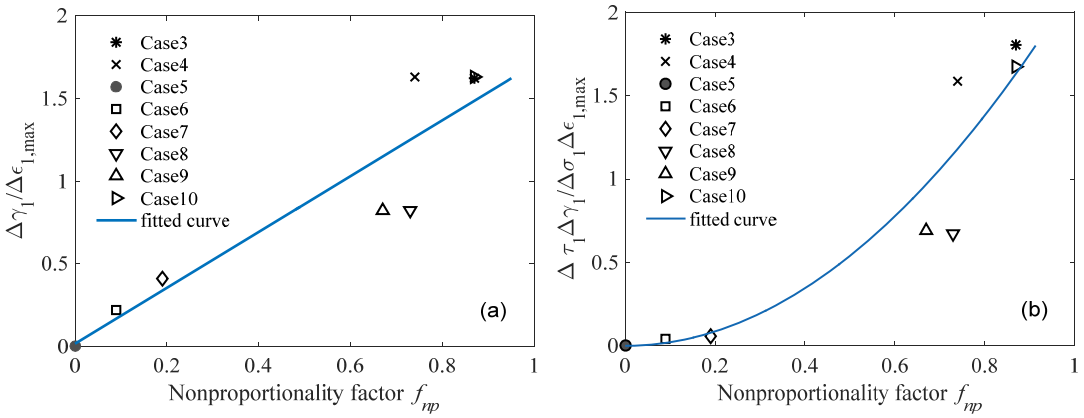

Fig. 5 Correlations between the non-proportionality factor and the parameters on the $\Delta\varepsilon_{1,\max}$ plane: (a) $\Delta\gamma_1/\Delta\varepsilon_{1,\max}$; (b) $\Delta\tau_1\Delta\gamma_1/\Delta\sigma_1\Delta\varepsilon_{1,\max}$

2.2 Determination of the critical plane for smooth thin-walled tube

As for the smooth thin-walled tube tested under tensional-torsional loadings, the stress and strain tensors on the tube surface can be expressed as:

$$\boldsymbol{\sigma}=\begin{bmatrix}\sigma_x & \tau_{xy} & 0\\ \tau_{xy} & 0 & 0\\ 0 & 0 & 0\end{bmatrix} \tag{16}$$

$$\boldsymbol{\varepsilon}=\begin{bmatrix}\varepsilon_x & \frac{1}{2}\gamma_{xy} & 0\\ \frac{1}{2}\gamma_{xy} & \varepsilon_y & 0\\ 0 & 0 & \varepsilon_z\end{bmatrix} \tag{17}$$

Based on Eqs. (16) and (17), the stresses and strains acting on the inclined plane (see Fig. 6) which make an angle α with the axis of the tube can be determined by[1]:

$$\sigma_\alpha=\frac{\sigma_x}{2}+\frac{\sigma_x}{2}\cos(2\alpha)+\tau_{xy}\sin(2\alpha) \tag{18}$$

$$\tau_\alpha=\frac{\sigma_x}{2}\sin(2\alpha)-\tau_{xy}\cos(2\alpha) \tag{19}$$

$$\varepsilon_\alpha=\frac{\varepsilon_x+\varepsilon_y}{2}+\frac{\varepsilon_x-\varepsilon_y}{2}\cos(2\alpha)+\frac{\gamma_{xy}}{2}\sin(2\alpha) \tag{20}$$

$$\frac{\gamma_\alpha}{2}=\frac{\varepsilon_x-\varepsilon_y}{2}\sin(2\alpha)-\frac{\gamma_{xy}}{2}\cos(2\alpha) \tag{21}$$

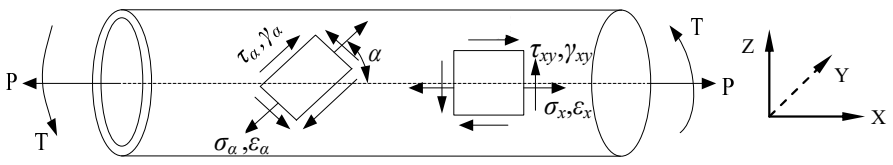

Fig. 6 Schematic diagram of the strains and stresses of tube specimen under tensional-torsional loading

The steps for determining the plane of maximum normal strain range are as follows:

1) Determine the strain and stress tensors at different times in the stabilized state. The best method to determine stress and strain tensors is through experimental testing. However, experimental testing is not only expensive but also time-consuming. Normally, the stress and strain tensors were determined by either a multiaxial constitutive model or finite element analysis.

2) Calculate the normal strain acting on the ith candidate plane with the inclined angle α_i using Eq. (20) at different times. Then, the normal strain range can be calculated by:

$$\Delta\varepsilon_{1,\alpha_i} = \max\left(\varepsilon_{\alpha_i}(j)\right) - \min\left(\varepsilon_{\alpha_i}(j)\right) \tag{22}$$

where j = 1, 2, 3, …, s_d. s_d is the subdivision's number in one applied loading cycle. That is to say, the applied loading cycle is divided into s_d subdivisions with a small time step.

3) Change α from 0° to 180° step-by-step with a small interval such as 0.1° and calculate the normal strain range acting on each inclined plane using Eq. (22). Among these planes, the critical plane is defined as the one which has the maximum normal strain range. Then, the location of the critical plane, i.e., the inclined angle α_{cr}, can be determined.

4) Calculate shear strain range, shear stress range, mean shear stress, and maximum normal stress acting on the critical plane by using the following equations:

$$\Delta\gamma_1 = \max\left(\gamma_{\alpha_{cr}}(j)\right) - \min\left(\gamma_{\alpha_{cr}}(j)\right) \tag{23}$$

$$\Delta\tau_1 = \max\left(\tau_{\alpha_{cr}}(j)\right) - \min\left(\tau_{\alpha_{cr}}(j)\right) \tag{24}$$

$$\tau_{1,m} = \frac{\max\left(\tau_{\alpha_{cr}}(j)\right) + \min\left(\tau_{\alpha_{cr}}(j)\right)}{2} \tag{25}$$

$$\sigma_{1,\max} = \max\left(\sigma_{\alpha_{cr}}(j)\right) \tag{26}$$

3. VALIDATION OF THE ESTABLISED CRITERION

Eight metallic materials tested under various loading paths were taken from literature[51, 57-64] to validate the prediction accuracy of the N-SWT model. The loading paths taken into account in the present study were illustrated in Fig. 7. The eight kinds of metals include 16MnR steel,[51] 7075-T651 aluminum alloy,[57] 1%Cr-Mo-V steel,[58] 30CrNiMo8HH steel,[59-60] SA 333 Gr.6 steel,[61] Q235B steel,[62] 2024-T3 aluminum alloy,[63] and 30CrMnSiA steel.[64] The reason

for selecting 30CrMnSiA steel is that it has been extensively tested under various loading conditions, including both proportional and non-proportional loading paths with normal and shear mean stresses. The other seven materials were selected based on the following criteria: (i) the loading conditions including both proportional and non-proportional loading paths, (ii) both the normal and shear stress ranges were measured, which can be utilized to verify the reliability of the plasticity model used in the present study, and (iii) the material constants contained in the considered life prediction models can be determined.

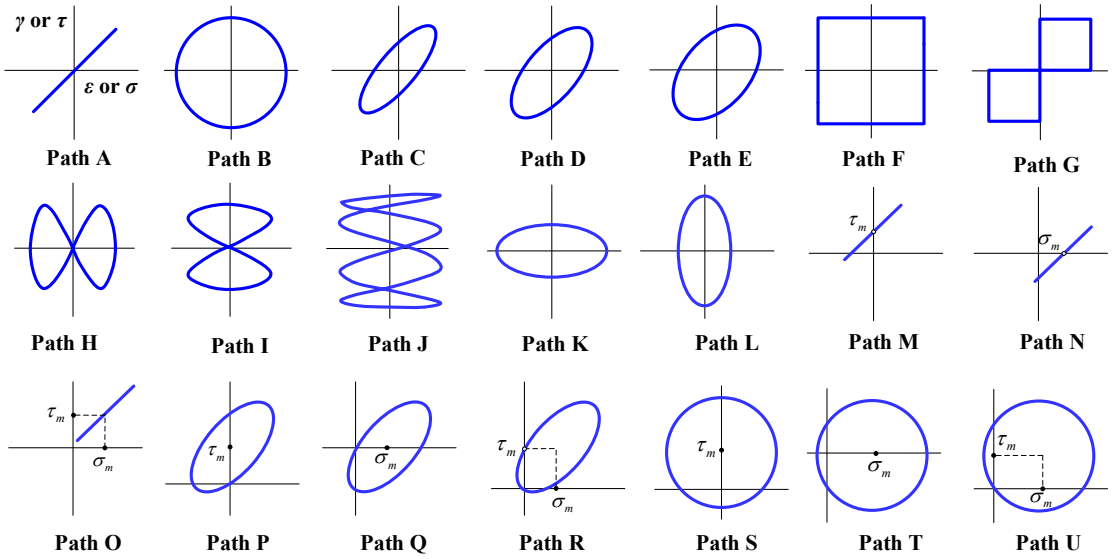

Fig. 7 Loading paths for the considered metallic materials[51, 57-64]

All the tests, except for 30CrMnSiA steel and 2024-T3 aluminum alloy, were performed in strain-controlled loadings by testing smooth thin-walled tubes at ambient temperature. As for the two materials, the tests are load-controlled. Symmetric multiaxial cyclic loadings were performed by Gates and Fatemi[63] on 2024-T3 aluminum alloy with smooth thin-walled specimens. However, asymmetric multiaxial cyclic loadings were conducted on 30CrMnSiA steel to study the influences of shear and normal mean stresses on fatigue life.[58] Besides, solid cylindrical specimens were utilized for 30CrMnSiA steel.

The specimen geometries and dimensions for the eight considered materials were presented in Fig. 8. The fatigue and monotonic properties of the considered metals were tabulated in Table 1. In this table, S_u and S_y represent the ultimate tensile strength and yield strength, respectively.

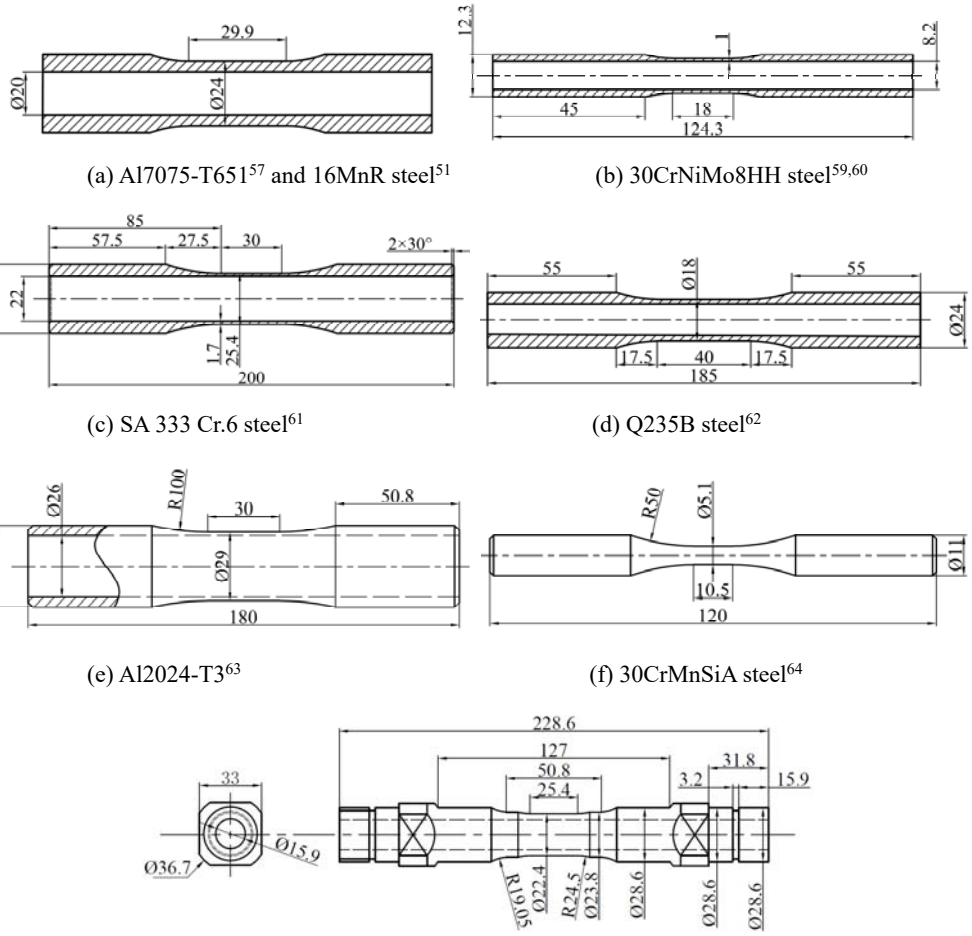

(a) Al7075-T651[57] and 16MnR steel[51] (b) 30CrNiMo8HH steel[59,60]

(c) SA 333 Cr.6 steel[61] (d) Q235B steel[62]

(e) Al2024-T3[63] (f) 30CrMnSiA steel[64]

(g) 1%Cr-Mo-V steel[58]

Fig. 8 Specimens for the considered metallic materials (all dimensions in *mm*)

Table 1 Monotonic and fatigue properties of the considered materials[51, 57-64]

	[a] 7075-T651[57]	[a] 1%Cr-Mo-V[58]	[b] 30CrNiMo8HH[59,60]	[a] 16MnR[51]	[a] SA 333 Gr.6[61]	[b] Q235B[62]	[b] 2024-T3[63]	[c] 30CrMnSiA[64]
Monotonic properties								
E (GPa)	71.7	208.0	200.0	212.5	203.0	204.0	73.4	207
G (GPa)	27.5	81.0	80.0	81.1	78.5	81.4	27.4	77.2
S_u (MPa)	561.0	805.0	1025.0	544.5	463.0	390.1	495.0	1334
S_y (MPa)	501.0	580.0	870.0	324.4	307.0	269.0	330.0	1196
v_e	0.306	0.29	0.3	0.31	0.3	0.3	0.343	0.34
Fatigue properties								
σ'_f (MPa)	1103.0	929.1	946.1	966.5	921.0	407.6	1194.0	1869.2
ε'_f	2.133	0.806	1.050	0.842	0.392	0.809	0.0660	0.244
b	-0.118	-0.0571	-0.0404	-0.101	-0.124	-0.0424	-0.133	-0.09
c	-1.056	-0.752	-0.732	-0.618	-0.532	-0.583	-0.445	-0.56
K' (MPa)	807.0	897.4	1617.0	1106.0	1015.0	642.2	677.0	2345.8
n'	0.0683	0.067	0.135	0.186	0.211	0.160	0.070	0.161
[d] w	0.426	0.721	0.677	0.773	0.789	0.804	0.465	0.50
[e] k_{FS}	0.3	1.1	1.0	1.0	0.7	1.3	1.0	1.0
Loading paths								
	A, B, I, J	A ~ D, K, L	A ~ H	A, B	A, B, D, K, L	A, B	A, B	M ~ U

[a] The fatigue properties were obtained by fitting the experimental results listed in the original literature.

[b] The fatigue properties were taken from the original literature.

[c] The fatigue properties were determined using the approximation method proposed by Roessle and Fatemi, [65] and the n' and K' were calculated using the compatibility equations.

[d] For 7075-T651, the Walker exponent w was determined by fitting the experimental results using the procedures proposed by Dowling.[49] For 2024-T3, the Walker exponent w was taken from reference.[16] For 30CrMnSiA, the Walker exponent w was determined by Eq. (3). For the other materials, the Walker exponent w was determined by using the approximation method proposed by Dowling.[50]

[e] For 7075-T651 and 1%Cr-Mo-V, the values of k_{FS} were determined by using the data tested under uniaixal and pure torsional loadings. For 30CrMnSiA, the k_{FS} value was determined by using the aproxiamtion method proposed by Fatemi et al.[66,67] For the other materials, the values of k_{FS} were taken from the original literature.

It can be seen from Eq. (15), both shear and normal stress terms were introduced in the established criterion to reflect the influences of non-proportional additional hardening and mean stress. Hence, the constitutive model is necessary to determine the stable stress-strain responses for various loading paths. Here, the constitutive model proposed by Li and his co-workers[68] was utilized to calculate the stable stress-strain responses except 30CrMnSiA steel. As for 30CrMnSiA steel, the Hooke's law was used since all the experimental data fall within the elastic regime.[6, 64] It is necessary to point out here that other constitutive models, such as those proposed by Jiang et al.,[69-70] Chaboche,[71] and so on, can also be applied to calculate the responses of cyclic stress-strain. However, it should be noted here that it is not an easy task to determine the material constants of these models reasonably, and some benchmark tests are usually necessary.[72-73]

The multiaxial fatigue lives of the considered metallic materials were predicted using the N-SWT model. Comparisons between the test data and the estimated lives were plotted in Figure 9, which shows the prediction accuracy of multiaxial fatigue lives for the considered metallic materials using the N-SWT model. In this figure, the dashed lines represent the factor-of-three boundary, and the solid line represents the perfect life prediction. From Fig. 9, it is evident that the majority of the prediction results fall within the factor-of-three boundary, regardless of the presence of mean stresses in the loading paths.

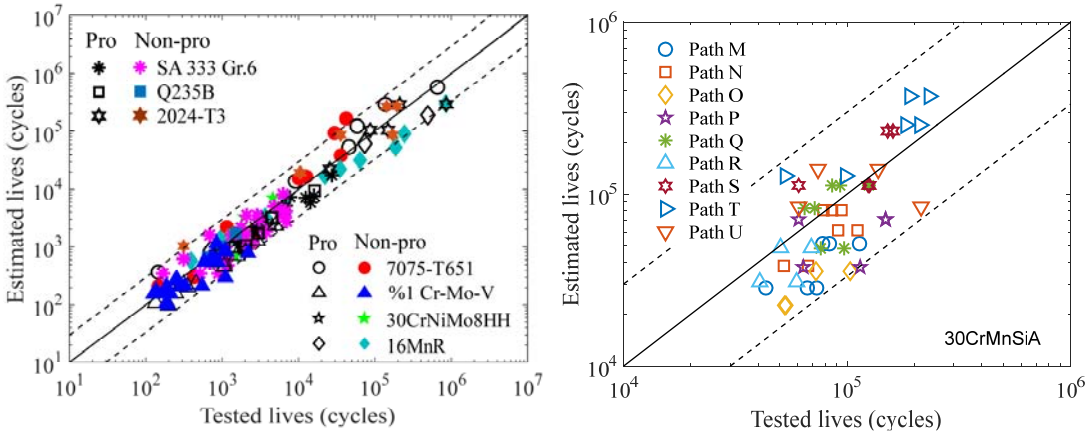

(a) the symmetric cyclic loading paths (b) the asymmetric cyclic loading paths

Fig.9 The tested fatigue lives vs. the estimated ones for the N-SWT model [51, 57-64]

In order to evaluate the prediction accuracy of the N-SWT model quantitatively, an error factor named as $E(s)$ was introduced. This error factor was defined as:

$$E(s)=\frac{\text{Number of data falling within}\ \frac{1}{s}\leqslant\frac{N_p}{N_t}\leqslant s}{\text{Number of total data}} \tag{27}$$

where N_p represents the predicted lifetime, and N_t represents the tested lifetime. $E(s)$ represents the percentage of data points that fall within the factor of "s" boundary. The prediction accuracy of the N-SWT model was listed in Table 2. It can be seen that, in cases where there are no mean stresses in the loading paths, approximately 79.3% of the data points fall within the factor-of-two boundary, indicating a relatively close agreement between the predicted and test fatigue lives. Moreover, an even higher percentage of the data points (about 96.8%) fall within the factor-of-three boundary, further reflecting the accuracy of the model in estimating multiaxial fatigue lives. For loading paths with mean stress, the prediction results are slightly lower but still within acceptable ranges. Specifically, around 72.9% of the data points fall within the factor-of-two boundary, and an encouragingly higher percentage of the data points (about 97.9%) fall within the factor-of-three boundary.

Table 2 The prediction accuracy of the considered life prediction models

Models	Without mean stress			With mean stress		
	$E(2)$	$E(3)$	$E(5)$	$E(2)$	$E(3)$	$E(5)$
N-SWT	0.793	0.968	1.0	0.729	0.979	1.0
SWT	0.509	0.690	0.832	0.541	0.687	0.791
CXH	0.748	0.929	0.993	0.416	0.708	0.895
FS	0.588	0.816	0.947	0.583	0.833	0.958

The probability analysis was applied using the prediction deviation, P_d to qualitatively describe the prediction accuracy of the established criterion. The expression of P_d is given as[74]:

$$P_d=\log_{10}\left(\frac{N_p}{N_t}\right) \tag{28}$$

Equation (28) indicates that non-conservative estimation will be obtained when the value of P_d is positive. When P_d equals to unity, perfect estimation can be obtained. The probability density function (PDF) which follows Gaussian distribution was selected, which can be expressed as:

$$f(x)=\frac{1}{\sqrt{2\pi}\delta}e^{-\frac{(x-\mu)^2}{2\delta^2}} \tag{29}$$

where μ represents the mean value, and δ represents the standard deviation. The fitted PDF for the P_d of different loading conditions was plotted in Fig. 10. The histograms of the prediction results under different loading paths were also shown in this figure, where the ordinate and abscissa are the values of frequency and P_d, respectively. Figure 10 shows that the N-SWT model generally provides good estimations for all the considered loading conditions. However, under proportional loading, the prediction results are slightly conservative.

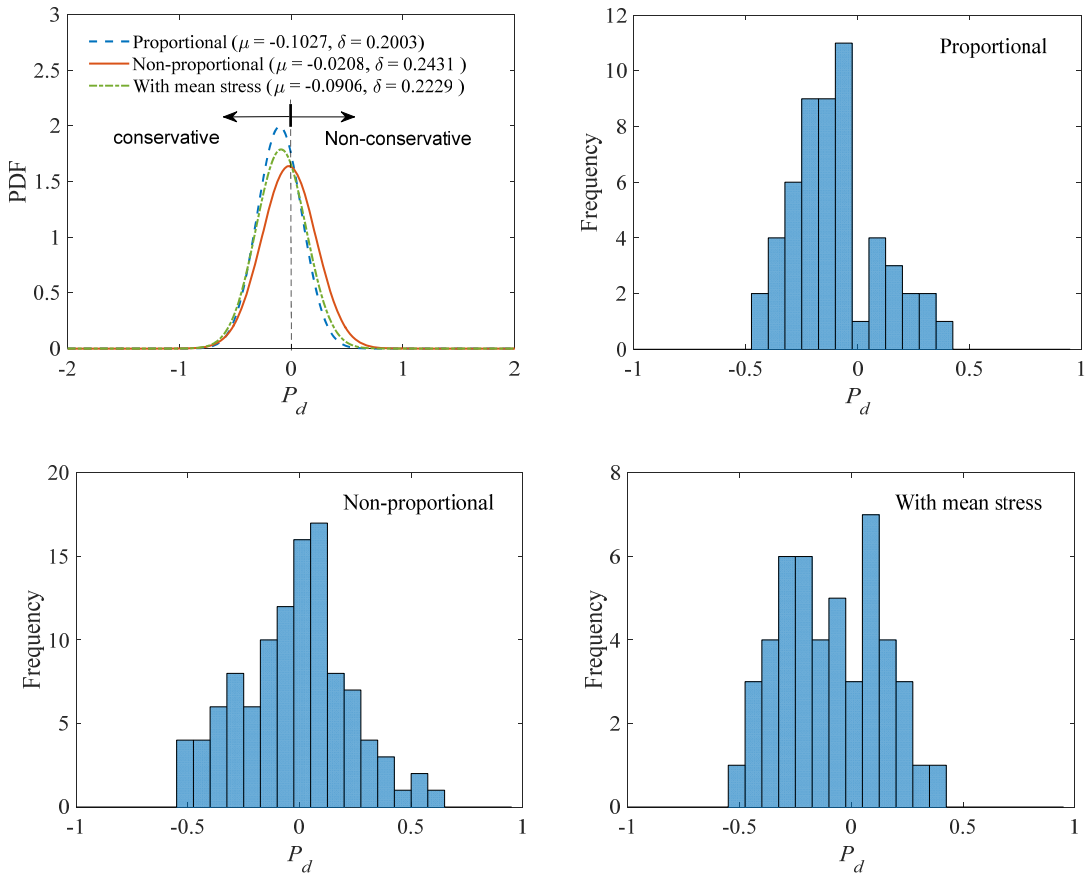

Fig. 10 Probability density functions and histograms of P_d for various loading conditions

4. DISCUSSIONS

As is known to all, the orientation of fatigue crack plays a crucial role in understanding the failure mechanism of a material under cyclic loading. Through experimental observations, the cracking behavior can be classified into three main categories, i.e., shear cracking, tensile cracking, and mixed cracking.[57] In the case of tensile cracking, the fatigue cracks are typically observed to propagate along the maximum normal strain/stress range plane.[57] For shear cracking, the fatigue cracks are often observed along the plane of maximum shear strain/stress

range.[57] A material may show mixed cracking behavior at the condition that the initiation of a fatigue crack is along the maximum normal strain/stress range plane during tension-compression loading while it is along the maximum shear strain/stress range plane during torsion loading.[57] The propagation direction of fatigue crack can be characterized by the angle between the crack growth plane and the axis of the specimen. According to the theory of the critical plane, the principal fatigue crack tends to propagate in or close to the critical plane.[43,75] The detailed procedures for comparing the predicted crack growth orientation with the experiments can be found in references.[43,75] The same as SWT model, the critical plane is defined as the maximum normal strain range plane in the proposed method. In theory, the proposed method is suitable for estimating the fatigue lifetime of a material experiencing Mode I failures (tensile cracking), which is analogous to the SWT model. In contrast, the FS model[44] is more suitable for the shear cracking since the critical plane is defined as the maximum shear strain range plane. Unfortunately, the cracking behavior of a material may not be determined before testing. In fact, Fatemi and Socie[44] have pointed out that the crack initiation and growth directions depend not only on the applied loading directions, but also on the type of material, loading stress/strain amplitude, and some others. The similar results were also observed by Zhao and Jiang.[57] Therefore, the N-SWT model may not be able to accurately predict the crack growth orientations for materials that exhibit shear cracking or mixed cracking behaviors.

Extensive multiaxial fatigue tests conducted over the last decades have indeed shown that there are reductions in fatigue life during non-proportional loadings compared to proportional loading at the same equivalent strain amplitude. As has mentioned above, Itoh et al.[52] performed a series of multiaxial fatigue tests on 304 stainless steel to show the loading path dependence of hardening. The loading paths have been plotted in Fig. 4. Correlation between the factor of non-proportionality and the maximum normal stress was plotted in Fig. 11. It can be seen that the maximum normal stress, $\sigma_{1,\max}$, increases with increasing the non-proportionality factor. Therefore, in the N-SWT model, the degree of non-proportionality can be taken into account by the maximum normal stress.

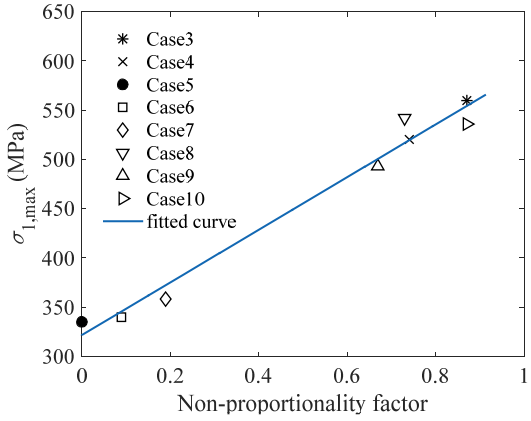

Fig.11 Correlation between the factor of non-proportionality and the maximum normal stress

It is important to note that strain-energy-density-based models, such as the SWT model, CXH model, etc., have advantages in accounting for the effects of non-proportional hardening on fatigue life because the stress terms were taken into account in these models. Besides that, the CXH model is another improved SWT model which was developed by Chen et al.[33] to provide better life predictions under non-proportional loadings. Therefore, in the present study, both the SWT and CXH models were chosen for validation and further comparison. The expressions of the SWT model and CXH model are given as:

SWT model:

$$\sigma_{1,\max}\frac{\Delta\varepsilon_{1,\max}}{2}=\frac{\sigma_f'^2}{E}\left(2N_f\right)^{2b}+\sigma_f'\varepsilon_f'\left(2N_f\right)^{b+c} \tag{30}$$

CXH model:

$$\frac{\Delta\sigma_1}{2}\frac{\Delta\varepsilon_{1,\max}}{2}+\frac{\Delta\tau_1}{2}\frac{\Delta\gamma_1}{2}=\frac{\sigma_f'^2}{E}\left(2N_f\right)^{2b}+\sigma_f'\varepsilon_f'\left(2N_f\right)^{b+c} \tag{31}$$

It is necessary to point out here that the CXH model can reduce to the SWT model under proportional loading. This is because under such conditions, there are no shear terms acting on the maximum normal strain range plane, and thus the CXH model simplifies to the SWT model. In fact, both the CXH model and the proposed one are modifications of the SWT model. If the compatibility assumption is ensured, i.e., the Coffin-Manson's plastic strain range and elastic strain range correlate with the correspondent Ramberg-Osgood's strain ranges perfectly, then the K' and n' can be determined by[76-79]:

$$n' = \frac{b}{c} \quad \text{and} \quad K' = \frac{\sigma'_f}{\varepsilon'^{\,b/c}_f} \tag{32}$$

Substitute Eq. (32) into Eq. (15), the N-SWT model can be rewritten as:

$$\sigma_{1,\max}^{\frac{1-w}{w}} \frac{\Delta\varepsilon_{1,\max}}{2} + \left(\frac{\Delta\tau_1}{2} + \left|\tau_{1,m}\right| \right)^{\frac{1-w}{w}} \frac{\Delta\gamma_1}{2} = \frac{\sigma'^{\,\frac{1}{w}}_f}{E} \left(2N_f\right)^{\frac{b}{w}} + \sigma'^{\,\frac{1}{w}-1}_f \varepsilon'_f \left(2N_f\right)^{\left(\frac{1}{w}-1\right)b+c} \tag{33}$$

Equation (33) shows that, if the value of w is set to 0.5, it can be observed that the N-SWT model reduces to the CXH model under centro-symmetric loading conditions.

For uniaxial loading condition, substitute Eq. (32) into Eq. (13), the established criterion can be rewritten as:

$$\sigma_{\max}^{1-w} \varepsilon_{a,t}^{w} = \sigma'_f \left(2N_f\right)^b \left[\frac{1}{E} + \frac{\varepsilon'_f}{\sigma'_f} \left(2N_f\right)^{c-b} \right]^w \tag{34}$$

It can be seen that the established criterion reduces to the SWT model as long as $w = 0.5$. If $w = 1$, Eq. (34) is seen to reduce to Eq. (6), and the established criterion coincides with the Coffin-Manson equation. If $w = 0$, Eq. (34) is rewritten as:

$$\sigma_{\max} = \sigma'_f \left(2N_f\right)^b \tag{35}$$

Equation (35) shows that the established criterion coincides with the Walker model in this condition.

Certainly, the FS model is another widely used critical-plane-based life prediction model. Hence, this model was also applied to compare with the other models in terms of their accuracy and reliability in predicting fatigue life. Different from the SWT and CXH models, the critical plane is defined as the plane of maximum shear strain range in FS model. The FS model can be expressed as:

$$\frac{\Delta\gamma_{\max}}{2} \left(1 + k_{FS} \frac{\sigma_{n,\max}}{\sigma_y} \right) = \left[\left(1+\nu_e\right) \frac{\sigma'_f}{E} \left(2N_f\right)^b + \left(1+\nu_p\right) \varepsilon'_f \left(2N_f\right)^c \right] \left(1 + k_{FS} \frac{\sigma'_f}{2\sigma_y} \left(2N_f\right)^b \right) \tag{36}$$

where $\Delta\gamma_{\max}$ and $\sigma_{n,\max}$ are the maximum shear strain range and the maximum normal stress on the critical plane, respectively. k_{FS} is a material constant which can be determined using the data tested under uniaxial and pure torsional fatigue loadings. ν_e and ν_p represent the elastic and plastic Poisson's ratios, respectively.

The metallic materials listed in Table 1 were also used to validate the prediction accuracy of the SWT model, CXH model, and FS model. The comparisons between the predicted lives and experimental ones for each model were shown in Fig. 12, Fig. 13, and Fig. 14, respectively. The dashed and solid lines in these figures also represent the factor-of-three boundary and the prefect prediction, respectively. Figures 12(a) and 13(a) show that both the SWT and CXH models can present satisfactory predictions under proportional loading. However, non-conservative prediction results were observed for SWT model under non-proportional loadings without mean stress since the shear components are not considered. By contrast, more reasonable prediction results were obtained by CXH model under the same loading paths. In more details, the prediction accuracy listed in Table 2 shows that 50.9% and 69% of data points predicted by SWT model fall within the factor-of-two and factor-of-three boundaries, respectively. As for the CXH model, 74.8% of the data points fall within the factor-of-two boundary, and 92.9% fall within the factor-of-three boundary. It means that $w = 0.5$ can simply be used in the N-SWT model for the absence of the tested Walker exponent. It should be pointed out here that a more accurate w value is still necessary to improve the prediction accuracy of the established criterion. Figure 14(a) shows that the FS model can also present satisfactory prediction results for proportional loading. However, under non-proportional loadings, the prediction results of FS model exhibit some scattering, although most of the data points still fall within the factor-of-three boundary. More specifically, 58.8% and 81.6% of the data points fall within the factor-of-two and factor-of-three boundaries, respectively.

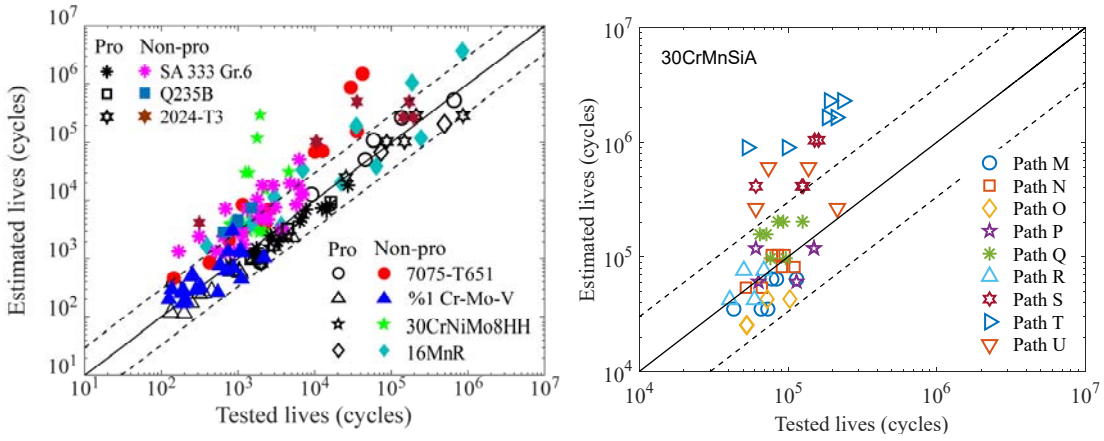

(a) the symmetric cyclic loading paths (b) the asymmetric cyclic loading paths

Fig.12 The tested fatigue lives vs. the estimated ones for the SWT model[51, 57-64]

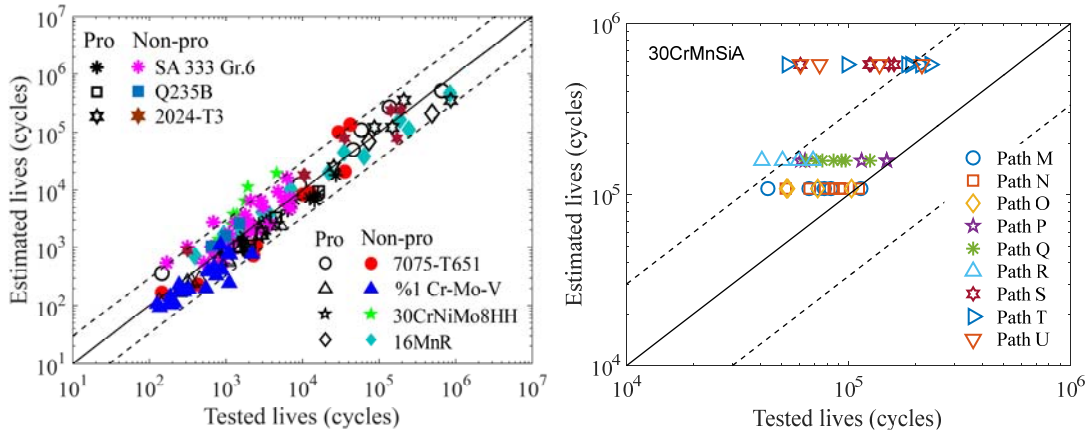

(a) the symmetric cyclic loading paths (b) the asymmetric cyclic loading paths

Fig.13 The tested fatigue lives vs. the estimated ones for the CXH model[51, 57-64]

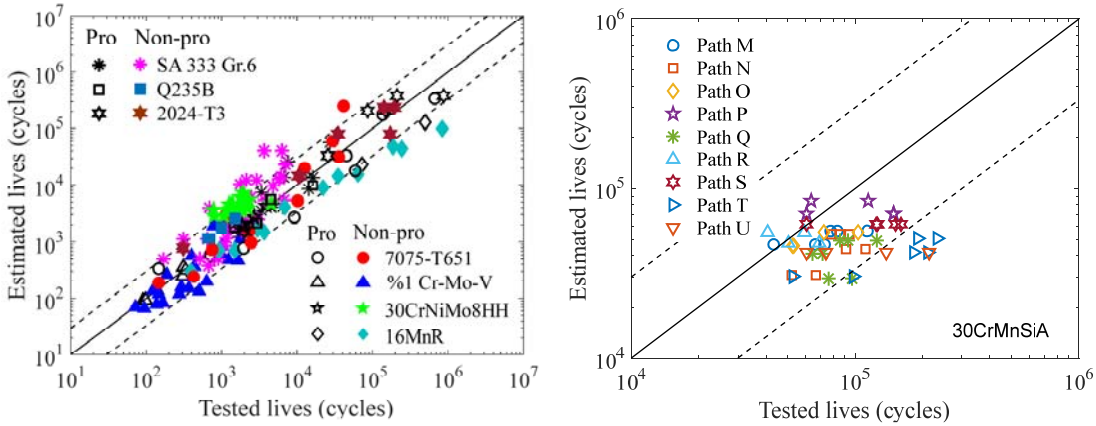

(a) the symmetric cyclic loading paths (b) the asymmetric cyclic loading paths

Fig.14 The tested fatigue lives vs. the estimated ones for the FS model[51, 57-64]

As for the loading paths with non-zero mean stress, Fig. 12(b) shows that the SWT model fails to give accurate estimations for assessing some of tested data of 30CrMnSiA steel. More exactly, the loading paths from M to R showed most of prediction results that fall within the factor-of-three boundary, which indicates good accuracy for these loading paths. However, non-conservative estimations were obtained for the paths from S to U. This could be attributed to the fact that paths S to U are circular loading paths with a high degree of non-proportionality, while paths M to R have a lower degree of non-proportionality. Based on Figs. 2, 3 and 5, it can be observed that the weight of shear strain energy density increases as the level of non-proportionality increases. For the loading paths with non-zero mean stress, the prediction accuracy listed in Table 2 shows that 54.1% and 68.7% of the data points predicted by the SWT model fall within the factor-of-two and factor-of-three boundaries, respectively. For the CXH model, according to Fig. 13(b), the prediction results are independent of

the non-zero shear/normal mean stress in the loading path, regardless of whether it is proportional or non-proportional loadings with the same loading stress amplitude. Hence, it appears that the same prediction results were obtained for paths M to O, paths P to R, and paths S to U in the CXH model. However, it is noted that the prediction results are unsatisfactory. The main reason for this unsatisfactory prediction is attributed to the model's neglect of the influence of mean stress on fatigue life. For the loading paths with non-zero mean stress, Table 2 shows that 41.6% and 70.8% of the data points estimated by CXH model fall within the factor-of-two and factor-of-three boundaries, respectively. As for FS model, Fig. 14(b) presents that most of the predicted lives are superior to the ones that estimated by SWT model and CXH model. However, it is also noted that for loading paths involving mean stresses, most of the data points were underestimated by the FS model. This suggests that the FS model may not accurately account for the influence of mean stress on fatigue life in these specific cases. In more details, 58.3% and 83.3% of the data points fall within the factor-of-two and factor-of-three boundaries, respectively. Compared with SWT, CXH and FS models, the N-SWT method can give more reasonable prediction results.

Figure 15 presents a box plot of P_d comparing the prediction accuracy of four models, namely the N-SWT model, SWT model, CXH model, and FS model. However, it is worth noting that Path A depicted in Fig. 8 was excluded from the box plot comparison. This exclusion is due to both the N-SWT model and CXH model reducing to the SWT model under proportional loading. According to Figure 15(a), it can be observed that the SWT model produces non-conservative prediction results under non-proportional loadings. Additionally, the fatigue life predictions generated by the FS model exhibit some scattering. In contrast, both the CXH model and N-SWT model demonstrate the ability to provide reasonable estimations. Further analysis has revealed that the prediction results of the N-SWT model are superior to those estimated by the CXH model. For asymmetric cyclic loading, Fig. 15(b) shows that almost all the prediction results of CXH model are non-conservative, while most of the predicted lives of FS model are conservative. The predictions of SWT model are the most scattered. In contrast to the three models, the established one displays the best estimations among the considered models. Overall, these results indicate that the N-SWT model performs well in predicting multiaxial fatigue lives for metallic materials, even when mean stresses are present

in the loading paths. It demonstrates the effectiveness and robustness of the N-SWT model in handling different loading conditions.

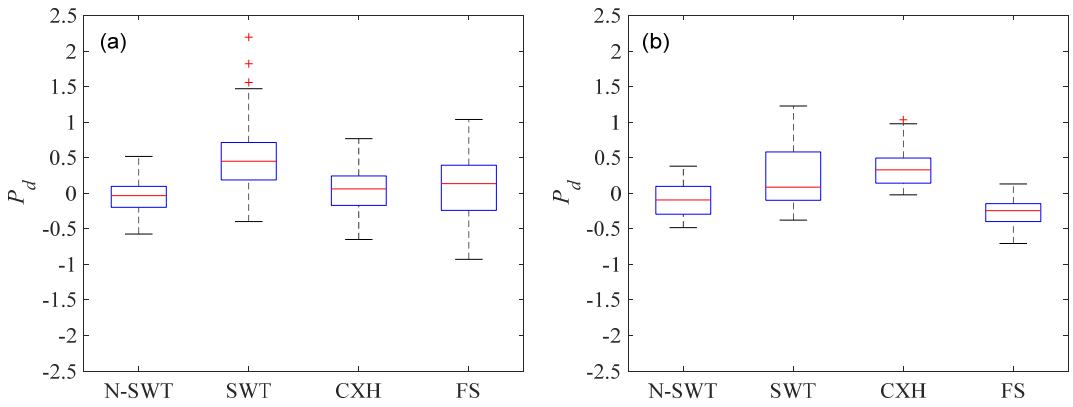

Fig. 15 Box plot of model prediction deviations: (a) non-proportional loadings, and (b) loading paths with mean stress

5. CONCLUSIONS

Among numerous fatigue life prediction methods, the SWT model has been widely used in fatigue life prediction, especially for materials that exhibit tensile cracking. However, it is often criticized for ignoring the influences of shear terms on fatigue damage, which may result in non-conservative prediction results during non-proportional loadings. Therefore, in this paper, an improved SWT model was developed by incorporating the equation of Walker into the strain-life curve. The prediction accuracy of the improved SWT model was validated using 8 kinds of materials. The prediction results were then compared with those obtained from the SWT model, CXH model, and FS model. Then, the conclusions can be drawn as follows:

(1) For symmetric cyclic loadings, the SWT model can provide reasonable predictions for fatigue life under proportional loading condition. However, it tends to yield non-conservative prediction results for non-proportional loadings. In contrast, the prediction results of FS model are somewhat scattered for these non-proportional loading paths, while the CXH model has shown to provide more accurate predictions.

(2) For the asymmetric cyclic loadings, the SWT, CXH, and FS models are all unable to accurately estimate the fatigue lifetime of the considered metals due to the influence of mean stress and/or non-proportionality. Specifically, the CXH model tends to provide non-conservative predictions, while the FS model tends to be conservative in predicting fa-

tigue life. The SWT model, on the other hand, produces the most scattered predictions.

(3) An improved SWT model was developed by incorporating the equation of Walker into the strain-life curve. Under uniaxial loading condition, when the value of w is set to 0.5, the established criterion is equivalent to the SWT model. When $w = 1$, the established criterion reduces to the Coffin-Manson equation. And when $w = 0$, the established criterion coincides with the Walker model. Under multiaxial loading conditions, the established criterion can reduce to the CXH model if the value of w is set to 0.5 and the loading paths are centro-symmetric. Experimental validation shows that the improved model can present satisfactory fatigue life predictions regardless of the presence of mean stress in the considered loading paths.

ACKNOWLEDGEMENTS

The authors gratefully acknowledge the financial support of the Natural Science Basic Research Program of Shaanxi (Program No. 2023-JC-YB-328), the National Natural Science Foundation of China (Program No. 12372328), the International Science and Technology Cooperation Program of Guangdong Province (2022A0505050047), and the Fundamental Research Funds for the Central Universities (Program No. ZYTS23014).

AUTHOR CONTRIBUTIONS

Jing Li: Conceptualization, Data curation, Methodology, Writing – Original draft, Writing – Review & editing. **Feng-shan Shao**: Writing – Original draft, Formal analysis, Validation. **Zheng-wei He**: Methodology, Investigation. **Juan Ma**: Supervision, Formal analysis. **Yuan-ying Qiu**: Funding Acquisition, Resources. **Michael Beer**: Writing – Review & editing.

CONFLICT OF INTEREST STATEMEN

The authors declare that they have no known competing financial interests or personal relationships that could have appeared to influence the work reported in this paper.

DATA AVAILABILITY STATEMENT

The data that support the findings of this study are available from the corresponding author upon reasonable request.

REFERENCES

[1] Socie DF, Marquis GB. Multiaxial Fatigue. Warrendale, PA: Society of Autonotive Engineering, 2000.

[2] Jordon BJ, Amaro R, Alllison P, Rao H. Fatigue in Friction Stir Welding. Amsterdam, Holland: Elsevier Science Publishing Company Inc., 2019.

[3] Matsubara G, Hayashida A, Kano D. Predicting the multiaxial fatigue limit and the multiaxial high-cycle fatigue life based on the unified equivalent shear stress from axial strength characteristics with various waveforms. International Journal of Fatigue, 2018;112:52-62.

[4] Susmel L, Lazzarin P. A bi-parametric Wöhler curve for high cycle multiaxial fatigue assessment. Fatigue & Fracture of Engineering Materials & Structures, 2002;25: 63-78.

[5] Zhang JL, Shang DG, Sun YJ, Wang XW. Multiaxial high-cycle fatigue life prediction model based on the critical plane approach considering mean stress effects. International Journal of Damage Mechanics, 2018;27:32-46.

[6] Li J, Wang X, Li K, Qiu YY. A modification of Matake criterion for considering the effect of mean shear stress under high cycle fatigue loading. Fatigue & Fracture of Engineering Materials & Structures, 2021;44:1760-1782.

[7] Carpinteri A, Spagnoli A, Vantadori S. Multiaxial fatigue assessment using a simplified critical plane-based criterion. International Journal of Fatigue, 2011;33:969-976.

[8] Wang XW, Shang DG, Sun YJ, Chen H. Multiaxial high-cycle fatigue life prediction model considering mean shear stress effect under constant and variable amplitude loading. Theoretical and Applied Fracture Mechanics, 2018;96:676-687.

[9] Susmel L. Notches, nominal stresses, fatigue strength reduction factors and constant/variable amplitude multiaxial fatigue loading. International Journal of Fatigue, 2022;162:106941.

[10] Li J, Qiu YY. A path-dependent multiaxial fatigue life estimation criterion for metals under various loading conditions. International Journal of Fatigue, 2021;149:106300.

[11] Kandil FA, Brown MW, Miller KJ. Biaxial low-cycle fatigue fracture of 316 stainless steel at elevated temperatures. London: The Metals Society; 1982. p. 203-210.

[12] Wang CH, Brown MW. A path independent parameter for fatigue under proportional and non-proportional loading. Fatigue & Fracture of Engineering Materials & Structures, 1993;16:1285-1298.

[13] Itoh T, Sakane M, Hata T, Hamada N. A design procedure for assessing low cycle fatigue life under proportional and non-proportional loading. International Journal of Fatigue,

2006;28:459-466.

[14] Zhong B, Wang YR, Wei DS, Wang JL. A new life prediction model for multiaxial fatigue under proportional and non-proportional loading paths based on the pi-plane projection. International Journal of Fatigue, 2017;102:241-251.

[15] Liu BW, Yan XQ. A new method for studying the effect of multiaxial strain states on low cycle non-proportional fatigue prediction. International Journal of Fatigue, 2018;117: 420-431.

[16] Meggiolaro MA, de Castro JTP. An improved strain-life model based on the Walker equation to describe tensile and compressive mean stress effects. International Journal of Fatigue, 2022;161:106905.

[17] Xiang D, Shen Y, Sun X. An energy-based approach for uniaxial fatigue life estimation under asymmetric cyclic loading. Fatigue & Fracture of Engineering Materials & Structures, 2023;46:2411-2423.

[18] Branco R, Prates P, Costa JD, Cruces A, Lopez-Cresop P. Berto F. On the applicability of the cumulative strain energy density for notch fatigue analysis under multiaxial loading. Theoretical and Applied Fracture Mechanics, 2022;120:103405.

[20] Li J, Wang X, Li RT, Qiu YY. Multiaxial fatigue life prediction for metals by means of an improved strain energy density-based critical plane criterion. European Journal of Mechanics / A Solids, 2021;90:104353.

[21] Ren Z, Qin X, Zhang Q, Sun Y. Multiaxial fatigue life prediction model based on an improved strain energy density criterion. International Journal of Pressure Vessels and Piping, 2022;199:104724.

[22] Benedetti M, Berto F, Le Bone L, Santus C. A novel Strain-Energy-Density based fatigue criterion accounting for mean stress and plasticity effects on the medium-to-high-cycle uniaxial fatigue strength of plain and notched components. International Journal of Fatigue, 2020;133:105397.

[23] Łagoda T, Vantadori S, Głowacka K, Kurek M, Kluger K. Using the Smith-Watson-Topper parameter and its modifications to calculate the fatigue life of metals: the state-of-the-art. Materials, 2022;15:3481.

[24] Socie D. Multiaxial fatigue damage models. Journal of Engineering Materials and Technology, 1987;109:293-298.

[25] Shlyannikov V, Ishtyryakov I, Yarullin R. Life-time prediction for aviation GTE compressor disk based on mixed-mode and multi-axial fracture resistance parameters. MATEC Web of Conferences, 2019;300: 11001.

[26] Deng PR, Matsumoto T. Fracture mechanics-based fatigue life prediction method for RC slabs in punching shear failure mode. Journal of Structural Engineering, 2020;146: 04019186.

[27] Noraphaiphipaksa N, Manonukul A, Kanchanomai C, Mutoh Y. Fretting fatigue life prediction of 316L stainless steel based on elastic-plastic fracture mechanics approach. Tribology International, 2014;78:84-93.

[28] Winkler A, Kloosterman G. A critical review of fracture mechanics as a tool for multiaxial fatigue life prediction of plastics. Frattura ed Integrità Strutturale, 2015, 33: 262-288.

[29] Cross R, Makeew A, Armanios E. Simultaneous uncertainty quantification of fracture mechanics based life prediction model parameters. International Journal of Fatigue, 2007;29:1510-1515.

[30] Pan J, Nicholas T. Effects of mean stresses on multiaxial fatigue life prediction based on fracture mechanics. International Journal of Fatigue, 2001;23:S87-S92.

[31] Jiang YY, Sehitoglu H. Fatigue and stress analysis of rolling contact. Report no. 161, UILU-ENG92-3602, College of Engineering, University of Illinois at Urbana-Champaign, 1992.

[32] Jiang YY. A fatigue criterion for general multiaxial loading. Fatigue & Fracture of Engineering Materials & Structures, 2000;23:19-32.

[33] Chen X, Xu S, Huang D. A critical plane-strain energy density criterion for multiaxial low cycle fatigue life under non-proportional loading. Fatigue & Fracture of Engineering Materials & Structures, 1999;22:679-686.

[34] Li J, Liu J, Sun Q, Zhang ZP, Qiao YJ. A modification of Smith-Watson-Topper damage parameter for fatigue life prediction under non-proportional loading. Fatigue & Fracture of Engineering Materials & Structures, 2012;35:301-316.

[35] Li J, Qiu YY, Tong XL, Gao L. A virtual-strain-energy-density-based critical-plane criterion to multiaxial fatigue life prediction. Journal of Materials Engineering and Performance, 2020;29:3913-3920.

[36] Lv Z, Huang HZ, Wang HK, Gao H, Zuo FJ. Determining the Walker exponent and developing a modified Smith-Watson-Topper parameter model. Journal of Mechanical Science and Technology, 2016;30:1129-1137.

[37] Walker K. The effect of stress ratio during crack propagation and fatigue for 2024-T3 and 7075-T6 aluminum. In: Effects of environment and complex load history on fatigue life. ASTM STP 462, Philadelphia, 1970, p. 1-14.

[38] Kujawski D. A deviatoric version of the SWT parameter. International Journal of Fatigue,

2014;67:95-102.

[39] Ince A, Glinka G. A generalized fatigue damage parameter for multiaxial fatigue life prediction under proportional and non-proportional loadings. International Journal of Fatigue, 2014,62:34-41.

[40] Ince A. A mean stress correction model for tensile and compressive mean stress fatigue loadings. Fatigue & Fracture of Engineering Materials & Structures, 2017;40:939-948.

[41] Yu ZY, Zhu SP, Liu Q, Liu Y. Multiaxial fatigue damage parameter and life prediction without any additional material constants. Materials, 2017;10:923.

[42] Li J, Wang X, Li RT, Qiu YY. Multiaxial fatigue life prediction for metals by means of an improved strain energy density-based critical plane criterion. European Journal of Mechanics / A Solids, 2021;90:104353.

[43] Poczklàn L, Polàk J, Kruml T. Comparison of critical plane models based on multiaxial low-cycle fatigue tests of 316L steel. International Journal of Fatigue, 2023;171:107565.

[44] Fatemi A, Socie DF. A critical plane approach to multiaxial fatigue damage including out-of-phase loading. Fatigue & Fracture of Engineering Materials & Structures, 1988;11:149-165.

[45] Nascimento V, Bemfica C, Fessler E, Araújo JA, Castro F. Multiaxial fatigue of forged Inconel 718 at room and high temperature, Theoretical and Applied Fracture Mechanics, 2022;122:103547.

[46] Branco R, Costa JD, Martins Ferreira JA, Capela C, Antunes FV, Macek W. Multiaxial fatigue behaviour of maraging steel produced by selective laser melting. Materials & Design, 2021;201:109469.

[47] Nourian-Avval A, Fatemi A. Fatigue performance and life prediction of cast aluminum under axial, torsion, and multiaxial loadings. Theoretical and Applied Fracture Mechanics, 2021;111:102842.

[48] Smith KN, Watson P, Topper TH. A stress-strain function for the fatigue of metals. Journal of Materials, 1970;5(4):767-778.

[49] Dowling NE. Mean stress effects in strain-life fatigue. Fatigue & Fracture of Engineering Materials & Structures, 2009;32:1004-1019.

[50] Dowling NE, Calhoun CA, Arcari A. Mean stress effects in stress-life fatigue and the Walker equation. Fatigue & Fracture of Engineering Materials & Structures, 2009;32: 163-179.

[51] Gao ZL, Zhao TW, Wang XG, Jiang YY. Multiaxial fatigue of 16MnR steel. Journal of Pressure Vessel Technology, 2009;131:021403.

[52] Kida S, Itoh T, Sakane M, Ohnami M, Socie DF. Dislocation structure and non-proportional hardening of type 304 stainless steel. Fatigue & Fracture of Engineering Materials & Structures, 1997;20:1375-1386.

[53] Meggiolaro MA, de Castro JTP. Prediction of non-proportionality factors of multiaxial histories using the moment of inertia method. International Journal of Fatigue, 2014;61:151-159.

[54] Wang CH, Miller KJ. The effect of mean shear stress on torsional fatigue behavior. Fatigue & Fracture of Engineering Materials & Structures, 2000;14:293-307.

[55] Wang XW, Shang DG, Sun YJ, Chen H. Multiaxial high-cycle fatigue life prediction model considering mean shear stress effect under constant and variable amplitude loading. Theoretical and Applied Fracture Mechanics, 2018;96:676-687.

[56] Chen YJ, Liu B, Liu CC. Multiaxial fatigue test of aeronautical aluminum alloys 2A12 and research on stress criterion life predictive model. China Mechanical Engineering, 2017;28:1092-1096 (in Chinese).

[57] Zhao TW, Jiang YY. Fatigue of 7075-T651 aluminum alloy. International Journal of Fatigue, 2008;30:834-849.

[58] Garud YS. Multiaxial fatigue of metals. Ph.D. Thesis, Stanford University, 1981.

[59] Noban M, Jahed H, Winkler S, Ince A. Fatigue characterization and modeling of 30CrNiMo8HH under multiaxial loading. Materials Science and Engineering A, 2011;528:2484-2494.

[60] Noban M, Jahed H, Ibrahim E, Ince A. Load path sensitivity and fatigue life estimation of 30CrNiMo8HH. International Journal of Fatigue, 2012;37:123-133.

[61] Arora P, Gupta SK, Bhasin V, Singh RK, Sivaprasad S, Tarafder S. Testing and assessment of fatigue life prediction models for Indian PHWRs piping material under multi-axial load cycling. International Journal of Fatigue, 2016;85:98-113.

[62] Qu WL, Zhao EN, Zhou Q, Pi YL. Multiaxial low-cycle fatigue life evaluation under different non-proportional loading paths. Fatigue & Fracture of Engineering Materials & Structures, 2018;41:1064-1076.

[63] Gates NR, Fatemi A. On the consideration of normal and shear stress interaction in multiaxial fatigue damage analysis. International Journal of Fatigue, 2017;100:322-336.

[64] Liu TQ, Shi XH, Zhang JY, Fei BJ. Multiaxial high-cycle fatigue failure of 30CrMnSiA steel with mean tension stress and mean shear stress. International Journal of Fatigue, 2019;129:105219.

[65] Roessle ML, Fatemi A. Strain-controlled fatigue properties of steels and some simple

approximations. International Journal of Fatigue, 2000;22:495-511.

[66] Shamsaei N, Fatemi A. Effect of hardness on multiaxial fatigue behavior and some simple approximations for steels. Fatigue & Fracture of Engineering Materials & Structures, 2009;32:631-646.

[67] Fatemi A, Shamsaei N. Multiaxial fatigue: An overview and some approximation models for life estimation. International Journal of Fatigue, 2011;33:948-958.

[68] Li J, Li CW, Zhang ZP. Modeling of stable cyclic stress-strain responses under non-proportional loading. Zeitschrift fur Angewandte Mathematik und Mechanik 2018;98:388-411.

[69] Jiang YY, Sehitoglu H. Modeling of cyclic ratchetting plasticity, part I: development of constitutive relations. Journal of Applied Mechanics, 1996;63:720-725.

[70] Jiang YY, Sehitoglu H. Modeling of cyclic ratchetting plasticity, part I: comparison of model simulations with experiments. Journal of Applied Mechanics, 1996;63:726-733.

[71] Chaboche JL. Time-independent constitutive theories for cyclic plastic. International Journal of Plasticity, 1986;2:149-188.

[72] Jiang YY, Kurath P. Characteristics of the Armstrong-Frederick type plasticity models. International Journal of Plasticity, 1996;12:387-415.

[73] Jiang YY, Zhang JX. Benchmark experiments and characteristic cyclic plasticity deformation. International Journal of Plasticity, 2008;24:1481-1515.

[74] Zhou J, Tan ZC, Cao LW, Wang YX. An improved critical plane-energy multiaxial fatigue life prediction model considering shear mean stress. Journal of Mechanical Science and Technology, 2023;37:1-9.

[75] Bemfica C, Carneiro L, Mamiya EN, Castro FC. Fatigue and cyclic plasticity of 304L stainless steel under axial-torsional loading at room temperature. International Journal of Fatigue, 2019;125:349-361.

[76] Niesłony A, Dsoki C, Kaufmann H, Krug P. New method for evaluation of the Manson–Coffin–Basquin and Ramberg–Osgood equations with respect to compatibility. International Journal of Fatigue, 2008;30:1967-1977.

[77] Li J, Zhang ZP, Sun Q, Li CW, Li RS. A simple relationship between axial and torsional cyclic parameters. Journal of Materials Engineering and Performance, 2011;20: 1289-1293.

[78] Li J, Zhang ZP, Li CW. An improved method for estimation of Ramberg-Osgood curves of steels from monotonic tensile properties. Fatigue & Fracture of Engineering Materials & Structures, 2016;39:412-426.

[79] Meggiolaro MA, de Castro JTP. Statistical evaluation of strain-life fatigue crack initiation predictions. International Journal of Fatigue, 2004;26:463-476.